photonics

MDPI

Article

Revolutionizing Firefighting: UAV-Based Optical Communication Systems for Wildfires

Mohammad Furqan Ali [1,2], Dushantha Nalin K. Jayakody [1,3,*] and P. Muthuchidambaranathan [4]

[1] COPELABS, Lusófona University, 1700-097 Lisbon, Portugal; mfurqan@autonoma.pt
[2] Centro de Investigação em Tecnologias—Autónoma TechLab, Universidade Autónoma de Lisboa, 1169-023 Lisbon, Portugal
[3] Department of Electrical & Electronics Engineering, Faculty of Engineering, Sri Lanka Institute of Information Technology, Malabe 10115, Sri Lanka
[4] Department of Electronics and Communications Engineering, National Institute of Technology, Tiruchirappalli 620015, India; muthuc@nitt.edu
* Correspondence: dushantha.jayakody@ulusofona.pt

Abstract: Wildfires are one of the most devastating natural disasters in the world. This study proposes an innovative optical wildfire communication system (OWC) that leverages advanced optical technologies for wildfire monitoring and seamless communication towards the 5G and beyond (5GB) wireless networks. The multi-input–multi-output (MIMO) optical link among communication nodes is designed by gamma–gamma (GG) distribution under consideration of intensity modulation and direct-detection (IM/DD) following an on–off-keying (OOK) scheme. In this study, the performance metrics of the proposed MIMO link that enables unmanned aerial vehicles (UAVs) are analytically derived. The end-to-end (E2E) performance metrics and the novel closed-form expressions for the average BER (ABER) and outage probability (P_{out}) are investigated for the proposed system models. Furthermore, the simulation results are obtained based on the real experimental data. The obtained results in this study are improved spatial resolution and accuracy, enabling the detection by communication of even small-scale wildfires at their inception stages. In the further perspective of this research, the development of the proposed system holds the potential to revolutionize wildfire prevention and control efforts, making a substantial impact on safeguarding ecosystems, communities, and economies from the devastating effects of fires.

Keywords: 5G and beyond (5GB) wireless optical network; MIMO-optical communication; optical communications; wildfire communication and detection; unmanned aerial vehicle (UAV) communication

check for updates

Citation: Ali M.F.; Jayakody, D.N.K.; Muthuchidambaranathan, P. Revolutionizing Firefighting: UAV-Based Optical Communication Systems for Wildfires. *Photonics* **2024**, *11*, 656. https://doi.org/10.3390/photonics11070656

Received: 10 May 2024
Revised: 3 July 2024
Accepted: 4 July 2024
Published: 11 July 2024

Copyright: © 2024 by the authors. Licensee MDPI, Basel, Switzerland. This article is an open access article distributed under the terms and conditions of the Creative Commons Attribution (CC BY) license (https://creativecommons.org/licenses/by/4.0/).

1. Introduction

In recent times, wildfires have become increasingly frequent due to global warming and environmental changes, posing significant threats to ecosystems and endangering numerous wildlife species. These events often result from high-temperature heat waves that ignite forest areas, causing extensive damage to natural resources, the environment, and our ecosystem. To mitigate these threats and protect wildlife, it is essential to develop an effective wildfire communication detection system. Traditional monitoring and planetary imaging systems are limited by their passive nature and inability to provide real-time data monitoring [1]. Enhancing the accuracy and efficiency of such systems can be achieved through the integration of an unmanned aerial vehicle (UAV) optical communication technique, which offers a promising solution for real-time observation and monitoring.

Unlike conventional radio frequency (RF) communication, the optical communication framework offers a secure, high-bandwidth, and interference-resistant alternative, enhancing situational awareness and firefighting strategies. The UAV wildfire optical communications (WOC) system incorporates advanced optical sensors, high-resolution

cameras, and laser communication devices mounted on UAV platforms. These state-of-the-art technologies enable UAVs to navigate challenging terrains, collect critical data swiftly, and communicate seamlessly with ground control centers and other UAVs. This integration facilitates a rapid and coordinated response to wildfire incidents, significantly boosting the operational capabilities of firefighting agencies in addressing these disasters with unprecedented efficiency.

The operational and deployment costs of UAVs are as nominal as those of aircraft and satellite imagery of higher costs. An additional benefit of deploying hovering UAVs at wildfire sites is the real-time communication combined with high-resolution imaging at low altitudes. It should be noted that the effective location and monitoring of wildfire sites are facilitated by the flexible movement of these hovering UAVs. The UAV-enabled communication system applies to burning warnings such as new confirmed fires emerging from affected wildfire locations [2].However, heat waves continuously increase temperature, and primary observation means that the heat waves offer an early warning of fires. Most recently, heat waves hit Europe which was the cause of the rising atmospheric temperature, placing forests at wildfire risk [3]. In particular, in Portugal during 2023, the two wildfire events occurred in Odemira and Ourem, which are 200 km and 140 m from the capital Lisbon [4]. However, the government authorities suspect and declare approximately 120 municipalities across Portugal at maximum risk of wildfires. The combination of scorching temperatures and very low humidity causes the water reservoirs to evaporate at a faster rate than in recent years. Therefore, an immediate call was required to find the wildfire sites before the events happened to save lives. Throughout this study, a wildfire UAV-enabled communication system is proposed (Figure 1).

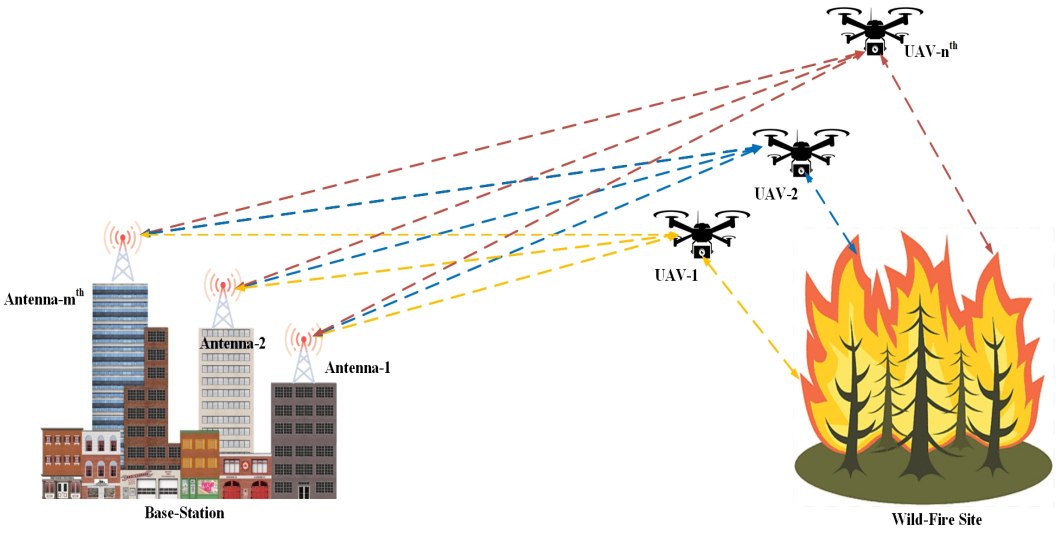

Figure 1. The proposed optical wildfire detection communication (OWDC) system model, where the *n*th of UAVs share the recorded data with the *m*th number of base stations (BSs). The GG distribution designs the whole communication system model to optimize channel turbulence.

The optical communication devices further enhance the system capabilities by facilitating rapid and secure data transmission, fostering seamless communication and collaboration among multiple UAVs and ground control centers [5,6]. An optical wireless communication (OWC) not only overcomes the shortcomings of traditional firefighting methods but also ushers in a new era of innovation in reducing the impact of wildfires on communities and ecosystems. At a glance, the UAVs provide remote virtual access to observe the affected sites. The UAV recorded data could be in real time, highly accurate in positioning at the affected site, and provide an emergency call for safety purposes [7,8]. Moreover, the mobility of UAVs allows for rapid and continuous video streaming of spread-

ing wildfires in forests. The deployment of multiple UAVs can be more profitable by scanning the affected area in multiple passes and incorporating base stations (BSs).

1.1. Literature Review

The most recent survey work discussed wildfire detection technologies [9], where the authors discussed the different UAV-enabled detection approaches. The advantageous deployment of UAVs offers the flexibility to reduce the cost, making it more suitable to reach remotely accessible recovery areas. A comprehensive study summarized the collaborative communication in a multi-UAV system [10]. The Internet of Things (IoT) network plays an important role in detecting wildfires. The role of the UAV-IoT futuristic wildfire detection system is highlighted, where the authors propose the discrete-time Markov chain (DTMC) method for fire detection in [11]. The challenges pose a threat of deploying the wildfire detection and management system to increase the frequency of wildfire detection systems. Therefore, the authors proposed a UAV-IoT-enabled wildfire detection system in [11]. Similarly, the authors in [12] proposed an optimized UAV wildfire monitoring and communication system algorithm in various fields. The authors in [13] investigated an optimal routing of the remote monitoring resources for a self-sufficient low-cost wildfire mitigation model (SL-PWR), which utilizes predicted spatiotemporal wildfire probability maps of the utility service area and optimized unmanned aerial vehicle (UAV) monitoring trees to obtain input images for training the SL-PWR modules. Correspondingly, an optimization unmanned aircraft system (UAS) model was developed to minimize the total amount of energy within the real-time data that must be transferred with the nearest base station [14].

On the other hand, an effective cooperative control framework for decision-making progress among the multiple agents is required. The authors in [15] proposed a cooperative control framework for a hierarchical UAV platform. However, this research included the greater possibilities of an optical wildfire detection communication system (OWDC) in real-time observation. The most recent work contains the three main aspects of early wildfire detection methodology and distance estimation for infrared images by utilizing UAV, such as in [16]. In [16], the authors targeted the smoke and suspected flame segmentation, wildfire spot distances, and infrared images for wildfire detection sites. In the extension of real-time data streaming of capturing images of wildfire sites, the authors in [17] proposed a deep learning model that transmits the affected site images collected by UAV to the base station for further analysis. Multi-UAV systems can offer a potential solution for wildfire detection and rescuing wildlife. Therefore, a multi-UAV wildfire detection framework was proposed to integrate sensing and operation in large-scale and dynamic wildfire environments [18].

Furthermore, this research work is organized as follows: the research work is proposed to reduce the complexity of the system by implementing the OOK scheme for its simplicity. The OOK scheme was chosen to improve the communication efficiency among transceivers rather than higher modulation techniques. The higher modulation techniques can be applicable in wildfire events but offer high complexity and cost, and affect communication efficiency. Therefore, the OOK scheme is adopted in this work. The proposed system model, channel coefficients, and communication links are designed by intensity modulation and direct detection (IM/DD), taking into account the OOK modulation/demodulation scheme in Section 2. The end-to-end (E2E) performance metrics such as average BER and outage probability are analytically derived in Section 3. The numerical parameters and simulation results based on experimental data are widely discussed in Section 4. Finally, the whole work is summarized in Section 5.

1.2. Main Contribution

Throughout this research work, we developed optical wildfire communication and monitoring systems using various UAV setups. The main contributions of this research are as follows:

- In this research, the development of the traditional wildfire communication technique is proposed to support real-time data streaming and rescue operations, improving video quality, and high-resolution imaging in wildfire sites. A quick response in real-time wildfire monitoring in remote areas by utilizing the unmanned aerial vehicles approach is proposed, as in [11]. An additional wildfire surveillance approach for early detection of remote sites and a quick response rather than satellite imaging and remotely operated drones was proposed in [19]. However, both of the existing works [11,19] lack the real experimental data-based MIMO wildfire optical approach for a very fast response in real-time monitoring. Therefore, our proposed scheme extended the existing wildfire approaches in real-time scenarios based on the experimental data. In addition to that, UAV-based wildfire communications are beneficial for sensing and capturing real-time data such as moisture, temperature, wind speed, etc., which could be further useful for the accurate prediction of fire spread rate. Therefore, the main contribution of this study is significantly important in the sphere of the provision in perspective of datasets.
- Our previous study of single-input–multi-output (SIMO) underwater visible light communication (UVLC) proposed a novel approach to signal transmission within moderate-to-strong turbulence channel conditions [20]. The SIMO-UVLC system is designed under consideration of gamma–gamma distribution towards the next generation of wireless networking systems. Therefore, this study extends and comprises the work in wildfire optical communication. This research proposes the diversity of optical communication within MIMO, MISO, SIMO, and SISO proposed communication models under strong turbulence channel conditions towards 5 GB wireless networking systems. It should be noted that the strong turbulence channel is designed taking into account the gamma–gamma distribution and the channel parameters α and β are calculated based on the real environmental data.
- The novel closed-form analytical expressions are derived from and comprise existing models. It is noteworthy that the path loss is deterministic, whereas the turbulence channel conditions are modeled by considering the random variables. Consequently, the proposed system is designed under intensity-modulation and direct-detection (IM/DD) following the OOK modulation/demodulation scheme.
- The evaluation of performance metrics, the average BER (ABER), and outage probability (P_{out}) of the proposed system models are well investigated and further simulated based on real-time experimental data. Performance metrics are depicted at different altitudes of UAVs. The experimental data are used based on the temperature, humidity, wind speed, and other environmental factors.

2. Wildfire Communication System Design

In this research, it is considered that the nth number of UAVs communicate with the mth number of monitoring base stations (BSs) through optical links within the harsh channel conditions. The proposed wildfire communication system model is depicted in Figure 1, where multiple UAVs transmit captured data from the affected site to the BS. It is obvious that the UAVs capture the wildfire data and transfer them to the BS, enabling combining methodology. It should be noted that each UAV can share information with an individual BS for a high probability of communication. The received signal at the BS within the multi-input–multi-output (MIMO) approach in full-duplex mode communication scenario toward the 5G and 6G wireless network is given as follows:

$$y_{nm} = r_{nm}\eta x \sum_{m=1}^{M} I_{nm} + \nu_{nm}, \tag{1}$$

where the parameters n and m represent the number of transmitted and receiver aperture within the IM/DD technique by following the on–off-keying (OOK) modulation/demodulation scheme. However, in this research, the parameters are considered as $m = n$ for equalization,

where $n, m = 1, 2, 3, \ldots N, M$, the responsivity of the photodetector is r_{nm}, the optical-to-electric conversion efficiency is η, the transmitted information symbol is x, and v_{nm} is the AWGN noise within the nm links of UAVs with zero means and the variance σ^2_{nm}, respectively. The normalized optical beam irradiance of nth transmitter to mth receiver is denoted by I_{nm}. It is noteworthy that I_{nm} is considered by implying the signal among nm communication nodes, where the path loss (I^t_{nm}) and atmospheric turbulence I^t_{nm} conditions are determined. Therefore, the combined channel conditions in terms of optical beam irradiance could be written as I_{nm}=$I^l_{nm} I^t_{nm}$, where I^l_{nm} is deterministic.

2.1. Managing Signal Power of UAV

Generally, optical communication links are widely defined based on the IM/DD approach. The simplicity of OOK modulation provides quite a significant suitability for UAV platforms, where the communication nodes consume high-energy constraints (P_{max}). However, it is necessary to maintain the linear relationship among the UAV nodes in their operational flight times. The optical powers received must not go beyond the threshold power (P_{min}) that produces a nonlinear effect. It is noteworthy that the transmitted average power (P_{avg}) is defined as $P_{min} \leq P_{avg} \leq P_{max}$.

In OOK modulation, for the power level (P_{enc}) of the encoding FSO signal, which maintains the linearity $[P_{max}, P_{min}]$ for constellation purpose, the selecting signal power level $\{P_c\}_{c=1}^{C}$ is written as $P_{min} \leq P_1, < P_2 ... < P_E \leq P_{max}$. Furthermore, in this proposed wildfire detection system model enabled by the FSO IMDD-OOK UAV, the selection of power levels (P_C) for the uniformity of distributed information $[P_{max} - P_{min}]$ can be written as follows:

$$P_C = P_{min} + \frac{c-1}{C-1}[P_{max} - P_{min}]; \quad c = 1, 2 \ldots C. \tag{2}$$

It is noteworthy that in this work the transmission power $P_1 = P_{min}$ for binary digit 0 and $P_2 = P_{max}$ for binary digit 1 is assigned. Therefore, the average power (P_{avg}) selection in IM/DD-OOK modulation technique of an individual UAV followed AWGN noise is written as follows:

$$P^{OOK}_{avg} = \frac{P_{max} + P_{min}}{2}. \tag{3}$$

Several challenges and solutions are associated with enabling wildfire management through scalable UAV-based communication systems. As the number of UAVs increases, bandwidth management becomes very important to avoid communication bottlenecks, with adaptive bandwidth allocation and hierarchical network designs being among the possible solutions. In the presence of dynamic environmental conditions and physical obstructions, there should be adaptive beam steering and multipath routing that will help maintain stable line-of-sight optical links (LOSs). The energy is also essential for a high probability of communication. It is noteworthy that the implementation of energy-efficient communication protocols can improve the system efficiency and quality of services. The base stations should be capable of handling increased data from several UAVs and necessitating scalable processing systems to prevent overload and latency. Simulations across various deployments under different environmental conditions can provide valuable insights into network performance, link stability, processing efficiency, and operational effectiveness.

The integration of UAV-based optical communication systems towards existing fire-fighting and emergency response infrastructure offers a transformative solution to wildfire management. By bridging the capabilities of satellites, ground sensors, and traditional networks, UAVs enhance overall situational awareness and operational efficiency. However, the satellites provide macro-level imagery data, but UAVs capture high-resolution imaging in real-time views, especially in those sites where satellites face limitations such as clouds and mountains. The ground-based sensors for localization environmental monitoring benefit from UAVs acting as mobile relays, extending the reach of sensor data to command centers, even when traditional infrastructure is compromised. Furthermore, UAVs can

augment and extend traditional communication networks by establishing ad hoc connections in remote areas, ensuring continuous and reliable communication among firefighting teams. This integration enables a robust, dynamic, and resilient response system, allowing for precise resource allocation, comprehensive monitoring, and adaptive coordination. The synergy between these advanced UAV systems and existing infrastructure ensures a multilayered defense against wildfires, enhancing both immediate response capabilities and long-term management strategies.

2.2. Approximated Path-Loss Channel Coefficient

In this study, the optical link is considered to be directly affected by the atmospheric conditions for fire data collection, the smoke of wildfire events, the capture of critical temperature, and detection activities. Due to harsh atmospheric channel conditions, the optical link severs attenuation in terms of extinction coefficient. Therefore, this study utilizes Beer Lambert's law [21] which is written as

$$\sigma_c^{nm}(\lambda) = \left(\frac{3.912}{V_{nm}}\right)\left(\frac{\lambda}{550}\right)^{-\delta}, \tag{4}$$

where the atmospheric extinction coefficient $\sigma_c^{nm}(\lambda)$ totally depends on optical-beam wavelength. The channel parameters, atmospheric visibility V (in km), and the size distribution coefficient of scattering δ, along with the distance L between n and m nodes, are considered [22]. Further, the path loss of each optical link is written as follows [23]:

$$I_{nm}^{l} = \exp[-\sigma_c^{nm}(\lambda)L]. \tag{5}$$

2.3. Turbulence Channel Conditions

In this research, the optical turbulence channel conditions are modeled under the gamma–gamma distribution model, which is a significant distribution for irregularities in the terrain, leading to multipath effects, and more suitable for optimizing the system performances [24]. The GG distribution is widely acknowledged as the most appropriate model for describing atmospheric turbulence in moderate to strong turbulence regimes [25]. Furthermore, the GG model is attractive from a performance analysis standpoint, particularly for MIMO FSO systems, where the distribution of the sum of independent GG variation needs to be determined. The GG distribution can provide more accurate results, especially in moderate to strong turbulence conditions. Additionally, the GG model works under all types of turbulence and offers better results [26]. The probability distribution function (PDF) of atmospheric turbulence channel conditions kth optical links of the proposed system model in terms of the generalized G-Meijer function is given as [27,28], where k is path links between nm nodes and the PDF for kth layer is written as follows:

$$f_{I_{t_k}}(I_{nm}) = \frac{\prod_{k=1}^{K}\Phi_{(\alpha_k\beta_k)}}{\prod_{k=1}^{K}\Phi_{(\Gamma\alpha_k\Gamma\beta_k)}} G_{0,2K}^{2K,0}\left[\prod_{k=1}^{K}\Phi_{(\alpha_k\beta_k)} I_{nm}\middle| \begin{matrix}\cdots \\ a_k\end{matrix}\right], \tag{6}$$

where $f_{I_{t_k}}(I_{nm})$ is the combined vector of nm communication nodes within kth layer, and the parameters are used in (6) along with the argument a_k as follows:

$$\prod_{k=1}^{K}\Phi_{(\alpha_k\beta_k)} = \left[\prod_{n,m=1}^{N,M}(\alpha)_{k,nm}\prod_{n,m=1}^{N,M}(\beta)_{k,nm}\right]$$

$$\prod_{k=1}^{K}\Phi_{(\Gamma\alpha_k\Gamma\beta_k)} = \left[\prod_{n,m=1}^{N,M}(\Gamma\alpha_k)_{n,m}\prod_{n,m=1}^{N,M}(\Gamma\beta_k)_{n,m}\right]$$

$$a_k = [(\alpha_1 - 1), \ldots (\alpha_k - 1), (\beta_1 - 1), \ldots (\beta_k - 1)]_{nm}$$

The large and small scale factors for the optical link can be written as [29]

$$\alpha_k = \left[\exp\left(\frac{0.49\sigma^2_{I_{t_k}}}{\left(1 + 0.18d^2 + 0.56\sigma^{\frac{12}{5}}_{I_{t_k}}\right)^{\frac{7}{6}}} \right) - 1 \right]^{-1}, \tag{7}$$

$$\beta_k = \left[\exp\left(\frac{0.51\sigma^2_{I_{t_k}}}{\left(1 + 0.9d^2 + 0.62d^2\sigma^{\frac{12}{5}}_{I_{t_k}}\right)^{\frac{5}{6}}} \right) - 1 \right]^{-1}. \tag{8}$$

For the optical link in (7) and (8), the scintillation index is denoted by $\sigma^2_{I_{t_k}}$, which is known as the Rytov variance and further calculated as $\sigma^2_{I_{t_k}} = 1.23{C_n}^2(h)\phi^{7/6}L^{11/6}$. However, in the Rytov variance, the number of optical waves is denoted by $\phi = 2\pi/\lambda$, which depends on the wavelength of the transmitted signal λ, and $d = 10D_r\sqrt{\frac{5\pi}{\lambda z}}$, along with the diameter of the receiver aperture D_r. The refraction index is described by C_n^2, which varies from $10^{-13}m^{-2/3}$ (for strong turbulence regime) to $10^{-17}m^{-2/3}$ (for weak turbulence regime) with uncertainties values at $10^{-15}m^{-2/3}$. Additionally, the Rytov variance associated with large-scale cells at $\sigma^2_{I_{t_k}} \gg 1$, while $\sigma^2_{I_{t_k}} \ll 1$ refers to small-scale cells taken into account by the plane wave model.

Generally, the refraction index is given as follows [30]:

$$C_n^2(h) = 0.00594(\frac{v}{27})^2(10^5h)^{10}\exp(-h/1000) + 2.7 \times 10^{-16}\exp(-h/1500) + A\exp(-h/100), \tag{9}$$

where v is the wind speed, A represents the level of C_n^2, and h is the altitude of an individual UAV. It is noteworthy that the outage performance is obtained based on varying altitudes for analysis as h = 25 m, 30 m, 35 m, and 40 m, respectively. However, in this study, the performance metrics are simulated at different altitudes of UAVs in Section 4.

The instantaneous electrical SNR $\gamma = (\eta r_{nm} I_{nm})^2/\sigma^2$ in relation to average electrical SNR could be written as $\overline{\mu} = (\eta|I_{nm}|)^2/\sigma^2$. Further normalizing $|I| = 1$ to utilize the average SNR $(\overline{\mu}) = \gamma/I^2_{nm}$ into (6), for equal gain, the PDF in terms of instantaneous SNR investigating the CDF is derived according to Appendix A:

$$f_{\gamma_k}(\gamma) = \frac{\prod_{k=1}^{K}\Phi_{(\alpha_k\beta_k)}}{2\sqrt{\gamma\overline{\mu}}\prod_{k=1}^{K}\Phi_{(\Gamma\alpha_k\Gamma\beta_k)}} G^{2K,0}_{0,2K}\left[\prod_{k=1}^{K}\Phi_{(\alpha_k\beta_k)}\sqrt{\frac{\gamma}{\overline{\mu}}}\middle| \begin{matrix} \cdots \\ \mathbf{a}_k \end{matrix}\right]. \tag{10}$$

To obtain the cumulative distribution function (CDF) of (6) as $F_{\gamma_k}(\gamma) = \int_0^{\gamma} f_{\gamma_k}(\gamma)d\gamma$, we utilized the properties of Wolfram Mathematica ([31], 07.34.21.0084.01) and obtained the expression in (11) as follows:

$$F_{\gamma_k}(\gamma) = \frac{2^{\sum_{k=1}^{K}(\alpha_k+\beta_k)-3K}\prod_{k=1}^{K}\Phi_{(\alpha_k\beta_k)}}{(2\pi)^K\prod_{k=1}^{K}\Phi_{(\Gamma\alpha_k\Gamma\beta_k)}}\sqrt{\frac{\gamma}{\overline{\mu}}}G_{1,4K+1}^{4K,1}\left[\prod_{k=1}^{K}\Phi_{(\alpha_k\beta_k)^2}\left(\frac{\gamma}{2^{4K}\overline{\mu}}\right)\middle|\begin{matrix}\frac{1}{2}\\ b_k,-\frac{1}{2}\end{matrix}\right]. \tag{11}$$

However, the argument b_k in (11) can be written as follows:

$$b_k = \left[\frac{\alpha_1-1}{2},\ldots\frac{\alpha_K-1}{2},\frac{\alpha_1}{2},\ldots\frac{\alpha_K}{2},\frac{\beta_1-1}{2},..\frac{\beta_K-1}{2},\frac{\beta_1}{2},\ldots\frac{\beta_K}{2}\right].$$

3. The End-to-End (E2E) Performances

This section includes the average BER and outage probability of the proposed MIMO-UAVs wildfire optical communication system. The performance metrics are obtained based on the real data given by Meteostat [32]. However, the outage performances and BER are the main insights used to depict the accuracy of the proposed wildfire communication system model.

3.1. Outage Probability of the Proposed System

To obtain the outage performance of the system, the instantaneous SNR should be equal to or less than the threshold SNR. Therefore, the outage probability performance could be written as follows:

$$P_{out} = F_{\gamma}(\gamma_{th}) = Pr\{\gamma \leq \gamma_{th}\}. \tag{12}$$

Furthermore, substituting (11) into (12), the outage probability of the proposed system is given as follows:

$$P_{out} = F_{\gamma}(\gamma_{th}) = \frac{Z_1\chi}{(2\pi)^K Z_{\Gamma(\alpha)\Gamma(\beta)}}\sqrt{\frac{\gamma}{\overline{\mu}}}G_{1,4K+1}^{4K,1}\left[\left(\frac{\gamma\chi^2}{2^{4K}\overline{\mu}}\right)\middle|\begin{matrix}\frac{1}{2}\\ b_k,-\frac{1}{2}\end{matrix}\right], \tag{13}$$

The parameters Z_1, $Z_{\Gamma(\alpha)\Gamma(\beta)}$, χ, and $Z_{\alpha\beta}$ are mentioned in Appendix A.

3.2. BER Performance Analysis

This subsection analytically summarizes the investigation of BER performance of the proposed system and comprises the possible communications as per the required MIMO, MISO, SIMO, and SISO system models. It is noteworthy that the proposed system models are designed under consideration of the moderate-to-strong turbulence channel conditions. Moreover, in this work, the closed-form expressions are analytically derived in consideration of the OOK modulation scheme under the IM/DD technique.

3.2.1. Analytical Performance of MIMO-FSO Detection System

To investigate the average BER, the number of UAVs is considered the equal number of UAVs at the BS, i.e., $m = n$. Therefore, the conditional BER in terms of average SNR ($\overline{\mu}$) for the MIMO system can be written as follows [33]:

$$\underbrace{P_{I_{nm}}}_{(MIMO)} = \frac{1}{2}erfc\left(\sqrt{\frac{\overline{\mu}}{2(NM)^2}\sum_{m=1}^{M}\left(\sum_{n=1}^{N}I_{nm}\right)^2}\right). \tag{14}$$

To form the closed-form expression of average BER within the combined turbulence and path loss conditions, the expression can be given as

$$\underbrace{\overline{BER}}_{MIMO} = \frac{1}{2}\int_0^{\infty} f_{I_{t_k}}(I_{nm}) erfc\left(\sqrt{\frac{\overline{\mu}}{2(NM)^2}\sum_{m=1}^{M}\left(\sum_{n=1}^{N} I_{nm}\right)^2}\right) dI_{nm}, \tag{15}$$

where $f_{I_{t_k}}(I_{nm})$ is the joint PDF of vector I=($I_{11}, I_{12}, \ldots I_{NM}$). The factors n and m indicate the transmitted and received power nodes at both communication ends. Furthermore, replacing (6) into (15) and converting the error function into a generalized G-Meijer function, we obtain (16), which is the complex integration expression. The expression (16) is a complex mathematical integration, therefore utilizing ([31], 07.34.21.0013.01), and we obtain the closed-form expression (17) of the proposed MIMO-FSO system model as follows:

$$\underbrace{\overline{BER}}_{MIMO} = \frac{\chi}{2\sqrt{\pi}Z_{\Gamma(\alpha)\Gamma(\beta)}}\int_0^{\infty} G_{0,2K}^{2K,0}\left[\chi I_{nm}\middle| \begin{matrix}\cdots \\ \mathbf{a}_{nm}\end{matrix}\right] G_{1,2}^{2,0}\left[\frac{\mu}{2(NM)^2}\sum_{m=1}^{M}\left(\sum_{n=1}^{N} I_{t_{nm}}\right)^2\middle| \begin{matrix}1 \\ 0, \frac{1}{2}\end{matrix}\right] dI_{nm}. \tag{16}$$

$$\underbrace{\overline{BER}}_{MIMO} = \frac{2^{\sum_{k=1}^{K}(\alpha_k+\beta_k)-2}}{Z_{\Gamma(\alpha)\Gamma(\beta)}\pi^{\left(\frac{2K+1}{2}\right)}} G_{4K+1,2}^{2,4K}\left[\frac{2^{4K-1}\mu}{(Z_{\alpha\beta}NM)^2}\middle| \begin{matrix}\Psi, 1 \\ 0, \frac{1}{2}\end{matrix}\right]. \tag{17}$$

In (17), the argument is given as follows:

$$\Psi = \left[\frac{(1-\alpha_1)}{2}, \ldots \frac{(1-\alpha_K)}{2}, \frac{(2-\alpha_1)}{2}, .. \frac{(2-\alpha_K)}{2}, \frac{(1-\beta_1)}{2}, \ldots \frac{(1-\beta_K)}{2}, \frac{(2-\beta_1)}{2}, \ldots \frac{(2-\beta_K)}{2}\right].$$

3.2.2. Analytical Performance of MISO-FSO Detection System

Similarly, in the investigation of the MISO-FSO system, the conditional BER for MISO and SIMO systems could be written by (18) according to (14). The conditional BER is written as follows:

$$\underbrace{P_{I_{nm}}}_{MISO} = \frac{1}{2} erfc\left(\sqrt{\frac{\overline{\mu}}{2M^2}\left(\sum_{m=1}^{M} I_m\right)^2}\right) \tag{18}$$

To obtain the closed-form expression of the MISO-FSO system, we plug (18) into (15) and further integrate by utilizing ([31], 07.34.21.0013.01). Therefore, the average BER analytical expression for MISO-FSO is obtained as in (19):

$$\underbrace{\overline{BER}}_{MISO} = \frac{2^{\sum_{k=1}^{K}(\alpha_k+\beta_k)-2}}{Z_{\Gamma(\alpha)\Gamma(\beta)}\pi^{\left(\frac{2K+1}{2}\right)}} G_{4K+1,2}^{2,4K}\left[\frac{2^{4K-1}\mu}{(Z_{\alpha\beta}M)^2}\middle| \begin{matrix}\Psi, 1 \\ 0, \frac{1}{2}\end{matrix}\right] \tag{19}$$

It is noteworthy that the argument Ψ is modified according to the required system model.

3.2.3. Analytical Performance of SIMO-FSO Detection System

This study follows the same pattern and plugs the conditional SIMO-FSO BER (20) into (15) and further integrates complex expression using ([31], 07.34.21.0013.01). The final average BER expression for the SIMO-FSO system is obtained by (21) as follows:

$$\underbrace{P_{I_{nm}}}_{SIMO} = \frac{1}{2} erfc\left(\sqrt{\frac{\overline{\mu}}{2N^2}\left(\sum_{n=1}^{N} I_n\right)^2}\right) \tag{20}$$

$$\underbrace{\overline{BER}}_{SIMO} = \frac{2^{\sum_{k=1}^{K}(\alpha_k+\beta_k)-2}}{Z_{\Gamma(\alpha)\Gamma(\beta)}\pi^{\left(\frac{2K+1}{2}\right)}} G_{4K+1,2}^{2,4K}\left[\frac{2^{4K-1}\mu}{(Z_{\alpha\beta}N)^2}\middle| \begin{matrix}\Psi, 1\\ 0, \frac{1}{2}\end{matrix}\right] \tag{21}$$

3.2.4. Analytical Performance of SISO-FSO Detection System

A single-input and single-output (SISO) is a generic communication system model with less complexity. In the SISO wildfire detection system, it is considered a single UAV that communicates with a single antenna or $n = m = 1$. Therefore, channel parameters are determined and modeled according to the single path with varying environmental factors. Due to the singularity of the communication nodes, the average BER is analytically derived in (22) as follows:

$$\underbrace{\overline{BER}}_{SISO} = \frac{2^{\alpha+\beta-2}}{\pi^{3/2}\gamma(\alpha)\Gamma(\beta)} G_{5,2}^{2,4}\left[\frac{4\mu}{(\alpha\beta)^2}\middle| \begin{matrix}\frac{1-\alpha}{2}, \frac{\alpha}{2}, \frac{1-\beta}{2}, \frac{\beta}{2}, 1\\ 0, \frac{1}{2},\end{matrix}\right]. \tag{22}$$

4. Numerical Evaluation and Simulation Results

In this section, the performance metrics of MIMO, MISO, SIMO, and SISO are simulated according to channel characteristics. However, we fixed the distance between the UAVs and the BS at 30 m, which could vary according to the requirements. Additionally, the results are generally depicted at the altitude of 25 m to 40 m of the UAV above ground level. The altitude can be increased according to the specific purpose or the requirement. However, the RF-enabled UAVs hover on higher altitudes rather than the optical-enabled UAVS. In this study, we considered the varying altitude of UAVs as 25 m, 30 m, 35 m, and 40 m to closely capture the affected site data. The UAVs are associated with optical links that can be easily affected by sunlight or any other environmental background. Therefore, we considered the fixed altitude for UAVs for more reliability and extension of this work. The average temperature, humidity, and pressure of July in Lisbon, Portugal, were taken for simulation results as $T = 22.56$ °C, 72.61 g/m^2, and $P = 1.016$ bar. The α and β particles are modeled based on the average atmospheric conditions under plan wave modulation and based on the refractive index C_n^2.

In Figure 2, the ABER performances are depicted on varying UAV altitude and BS while the other parameters are fixed as T = 22.5 °C and average humidity 72.61 g/m^3. It should be noted that the results were obtained taking into account the equal number of transmitters and receivers. It can be seen that with the increasing altitude of UAVs, the performances become poor. This is because of the harsh conditions in the channel on increasing height. However, the best ABER performances are depicted at $d = 25$ m of an individual UAV. If targeting 10^{-5} BER, the performances outperform in the 16 dB SNR regimes, while in the $d = 40$ regimes they are the poorest in the high-SNR regimes.

Figure 3 shows the performance of ABER on varying numbers of UAVs and BSs. Firstly, the results are obtained when increasing the number of BSs while the number of UAVs is kept constant. It can be seen that when increasing BSs the performance reduces simultaneously, while other parameters are fixed as $h = 25$ m and $d = 20$ m. On the other hand, if the number of UAVs increases, the performance improves significantly. This is because of the number of source nodes and the high probability of receiving signals from multiple communication nodes. It also includes the performance in equalizing the number of UAVs and the BSs, which could achieve the best performance. However, upon concluding these results, the ABER improves if it deploys an equal number of communication nodes. The distance between communication nodes and channel parameters influences the

performance metrics. Another way to obtain these results is when increasing the number of BSs, the performance reduces in high-SNR conditions. However, reducing the number of BSs improves within low-SNR regimes.

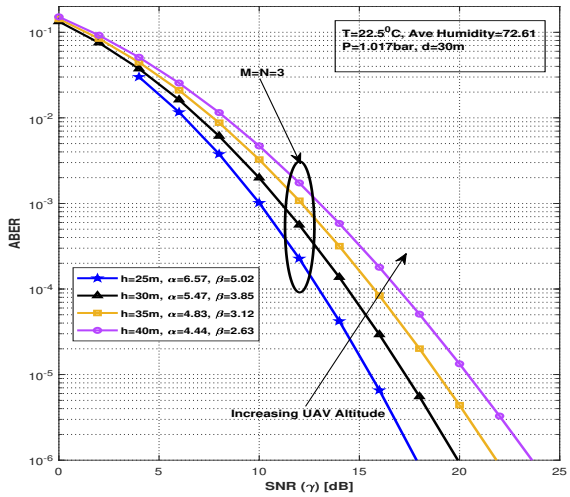

Figure 2. The ABER performances while varying the altitude of an individual UAV. In this figure, it is depicted clearly that with increasing UAV altitude the performance decreases.

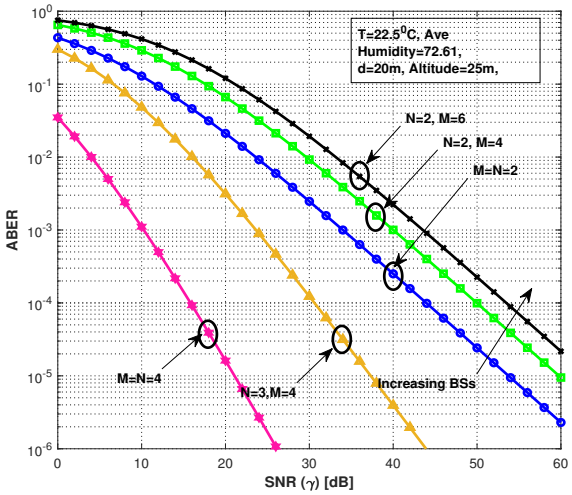

Figure 3. The ABER performance is obtained and comprises a fluctuating number of communication nodes. It is depicted that by increasing the number of UAVs, ABER performance improves simultaneously.

Upon continuous shifting parameters, Figure 4 shows the ABER performance of the proposed system model as MIMO, MISO, SIMO, and SISO wildfire detection. In this study, real data were used to depict the performance of the system. Therefore, the MIMO and MISO systems obtained superior performance compared to those of SIMO and SISO. The reason is discussed in Figure 3. Interestingly, the MISO detection system outperforms MIMO. According to Figure 3, it is shown that increased UAVs improve performance. The SIMO and SISO have less probability of multiple-node communication. Therefore, MIMO and MISO systems obtain higher ABER performance in low-SNR conditions compared to SIMO and SISO detection models.

Throughout Figure 5, the outage performance of the proposed system is depicted on successive threshold SNRs in strong turbulence channel conditions, when other parameters are kept fixed. It can be seen that as γ_{th} increases, the probability of the outage shows poor performance. It should be noted that the best performance is obtained at $\gamma_{th} = 2$ dB while the average performance is obtained at $\gamma_{th} = 6$ dB. In this figure, the numbers

of UAVs and BSs are kept equal for simulation results as $M = N = 2$, and the average temperature and humidity are taken as $T = 22.5$ °C and 72.61 g/m^2. However, the results are obtained at fixed communication distance and UAV altitude of $d = 30$ m and $h = 30$ m. The closed-form expression in (13) is used to obtain the simulation results.

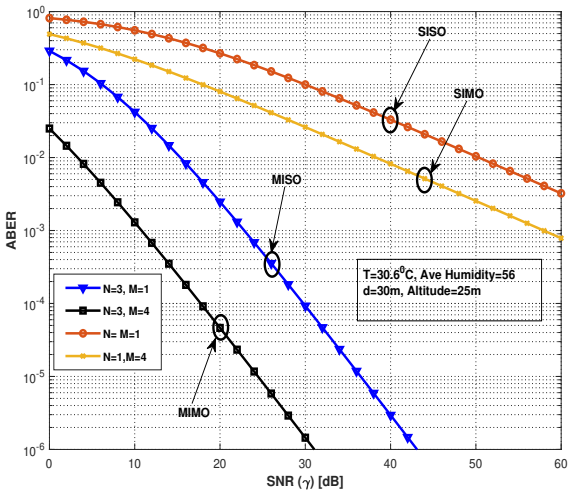

Figure 4. The ABER performance comparison among MIMO, MISO, SIMO, and SISO when the numbers of UAVs and BS vary. Moreover, the best ABER performance is depicted within MIMO and MISO wildfire detection systems.

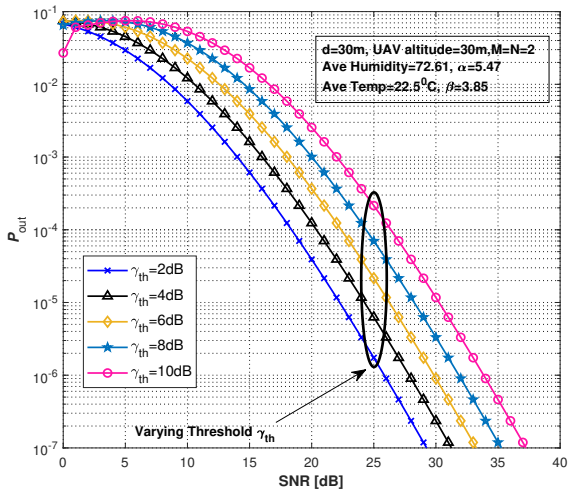

Figure 5. The outage performances are depicted on varying threshold SNR while the real-time data are used for July in Lisbon, Portugal. It is shown that the best performance is obtained at $\gamma_{th} = 2$ dB.

Finally, in Figure 6, the outage performance is depicted on varying UAV altitudes which vary from 25 m to 40 m above ground level. Similarly, increasing UAV altitude reduces the system performance and directly affects it, due to strong turbulence channel conditions. In this figure, the results are obtained at average temperature and humidity, as in Figure 5. The best performance is obtained at 25 m at the lowest SNR regimes because it is the shortest distance compared to other UAV altitudes.

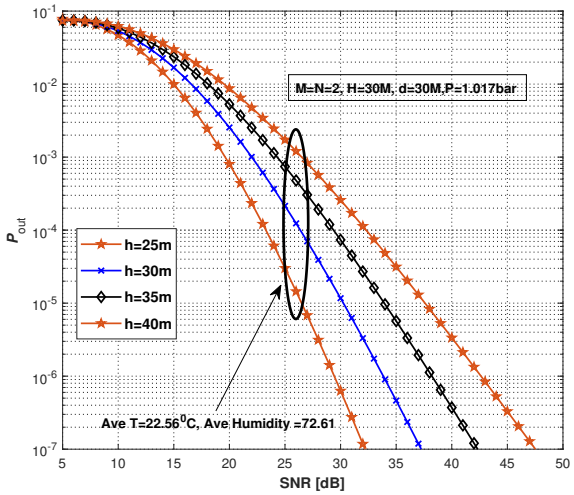

Figure 6. The outage probability performance for the successive altitude of UAV from the ground level while the other parameters are kept constant.

5. Conclusions

This research provides new insights into wildfire events by enabling UAV communication setups for real-time monitoring within the future wireless system. The MIMO optical-enabled UAV wildfire communication system represents a cutting-edge and highly efficient approach to early wildfire monitoring and response. In this work, the MIMO optical link among communication nodes is designed using the gamma–gamma distribution under the IM/DD-OOK modulation scheme. Furthermore, this study explores potential communication approaches in remote areas. The PDF and CDF are derived to obtain the system's performance metrics. This work aims to develop a wildfire communication model to save lives and support rescue operations. The results demonstrate improved spatial resolution and accuracy—this enables the detection of even small-scale wildfires at its inception stages. The proposed system's capability to provide real-time, accurate, and comprehensive wildfire monitoring will not only aid in the prompt observation of fire incidents but will also enhance life-saving and rescue operations. The development of this research signifies a revolution in wildfire monitoring and control efforts, substantially impacting the protection of ecosystems, communities, and economies from the devastating effects of wildfires.

Author Contributions: Conceptualization, M.F.A. and D.N.K.J.; methodology, M.F.A. and D.N.K.J.; validation, M.F.A.; formal analysis, M.F.A.; investigation, M.F.A.; resources, M.F.A., P.M. and D.N.K.J.; data curation, M.F.A.; writing—review and editing, P.M. and D.N.K.J.; supervision, D.N.K.J.; project administration, D.N.K.J. and P.M. All authors have read and agreed to the published version of the manuscript.

Funding: This work was supported, in part, by the Scheme for Promotion of Academic & Research Collaboration (SPARC) in India, via grant no. SPARC/2024-2025/NXTG/P3524, by the Sri Lanka Institute of Information Technology via PVC(R&I)/RG/2024/12, by the COFAC—Cooperativa de Formação e Animação Cultural, C.R.L. (University of Lusófona University), via the grant AOEE-WiPS (COFAC/ILIND/COPELABS/2/2022), and PortuLight (COFAC/ILIND/COPELABS/2/2023), by the national funds through FCT - Fundação para a Ciência e a Tecnologia—as part of the project AIEE-UAV (no. 2022.03897.PTDC), CEECINST/00002/2021/CP2788/CT0003 and COPELABS (no. UIDB/04111/2020).

Institutional Review Board Statement: This study was conducted according to the guidelines of the declaration of approval by the institutional review board of Lusófona University, Lisbon, Portugal.

Informed Consent Statement: Informed consent was obtained from all subjects involved in the study.

Data Availability Statement: The real data were taken from the city of Lisbon during the month of July 2023. The corresponding work is cited already the manuscript. https://meteostat.net/en/place/pt/alfragide?s=08535t=2023-07-22/2023-07-29. The data has been accessed and available online on 22 July 2023.

Conflicts of Interest: The authors declare no conflicts of interest.

Appendix A

Appendix A.1

We plug the instantaneous SNR $\gamma = \bar{\gamma} I^2$ into (6) in the terms of average SNR and obtain (10). Further, we integrating (10) to obtain CDF and analytical outage performance of the system as follows:

$$P_{out} = Pr\{\gamma \leq \gamma_{th}\} = F_{\gamma}(\gamma_{th}) \tag{A1}$$

The variables Z_1, $Z_{\Gamma(\alpha)\Gamma(\beta)}$, χ, and $Z_{\alpha\beta}$ in (13) are used as follows:

$$Z_1 = 2^{\sum_{k=1}^{K}(\alpha_k+\beta_k)-3K}, \quad \text{and} \quad \chi = \prod_{k=1}^{K} \Phi_{(\alpha_k\beta_k)}$$

$$Z_{\Gamma(\alpha)\Gamma(\beta)} = \prod_{k=1}^{K} \Phi_{(\Gamma\alpha_k\Gamma\beta_k)}, \quad \text{and} \quad Z_{\alpha\beta} = \prod_{k=1}^{K} \Phi_{(\alpha_k\beta_k)}.$$

Appendix B

The BER of the IM/DD within the OOK scheme in the presence of perfect CSI, at the receiver end, is given as $P_{error} = P(1)_{e|1} + P(1)_{e|0}$. The parameters $P(1)$ and $P(0)$ are associated with the probabilities of transmitting bits as 1 and 0. Therefore, the symmetrical problem and the probabilities can be written as $P(0) = P(1) = 0.5$ or $P(e|1) = P(e|0)$. The error probability for conditional irradiance I_{nm} is given [33] as follows:

$$P(e|I_{nm}) = P(e|1, I_{nm}) = P(e|0, I_{nm}) = \frac{1}{2} erfc\left(\frac{\eta I_{nm}}{\sqrt{2N_0}}\right) \tag{B2}$$

Therefore, the average BER can be written as follows:

$$\underbrace{\overline{BER}}_{MIMO} = \frac{1}{2} \int_0^{\infty} erfc\left(\frac{\eta I_{nm}}{\sqrt{2N_0}}\right) f_{I_{nm}} dI_{nm} \tag{B3}$$

Furthermore, we plug in the PDF from (10) as follows:

$$\underbrace{\overline{BER}}_{MIMO} = \frac{1}{2} \int_0^{\infty} f_{I_{t_k}}(I_{nm}) erfc\left(\sqrt{\frac{\overline{\mu}}{2(NM)^2} \sum_{m=1}^{M} \left(\sum_{n=1}^{N} I_{nm}\right)^2}\right) dI_{nm}. \tag{B4}$$

However, the above integration is complex to integrate. Therefore, utilizing the properties of the G-Meijer function from the integral table ([31], 07.34.21.0013.01), we obtain the final closed-form expression for BER as follows:

$$\underbrace{\overline{BER}}_{MIMO} = \frac{2^{\sum_{k=1}^{K}(\alpha_k+\beta_k)-2}}{Z_{\Gamma(\alpha)\Gamma(\beta)}\pi^{(\frac{2K+1}{2})}} G_{4K+1,2}^{2,4K}\left[\frac{2^{4K-1}\mu}{(Z_{\alpha\beta}NM)^2}\middle| \begin{matrix} \Psi, 1 \\ 0, \frac{1}{2} \end{matrix}\right]. \tag{B5}$$

References

1. Bouguettaya, A.; Zarzour, H.; Taberkit, A.M.; Kechida, A. A review on early wildfire detection from unmanned aerial vehicles using deep learning-based computer vision algorithms. *Signal Process.* **2022**, *190*, 108309. [CrossRef]
2. Allison, R.S.; Johnston, J.M.; Craig, G.; Jennings, S. Airborne optical and thermal remote sensing for wildfire detection and monitoring. *Sensors* **2016**, *16*, 1310. [CrossRef] [PubMed]
3. Rebecca Ann Hughes, EURO NEWS. Available online: https://www.euronews.com/green/2023/08/18/europe-is-heading-into-another-heatwave-here-are-all-the-areas-affected (accessed on 1 August 2023).
4. Reuter. Available online: https://www.reuters.com/world/europe/iberian-peninsula-braces-heatwave-wildfires-blaze-portugal-2023-08-07/ (accessed on 1 August 2023).
5. Zhu, L.; Zhang, J.; Xiao, Z.; Cao, X.; Wu, D.O.; Xia, X.G. 3-D beamforming for flexible coverage in millimeter-wave UAV communications. *IEEE Wirel. Commun. Lett.* **2019**, *8*, 837–840. [CrossRef]
6. Yi, P.; Zhu, L.; Xiao, Z.; Zhang, R.; Han, Z.; Xia, X.G. 3-D Positioning and Resource Allocation for Multi-UAV Base Stations Under Blockage-Aware Channel Model. *IEEE Trans. Wirel. Commun.* **2023**, *23*, 2453–2468. [CrossRef]
7. Zhu, L.; Zhang, J.; Xiao, Z.; Xia, X.G.; Zhang, R. Multi-UAV aided millimeter-wave networks: Positioning, clustering, and beamforming. *IEEE Trans. Wirel. Commun.* **2021**, *21*, 4637–4653. [CrossRef]
8. Zhu, L.; Zhang, J.; Xiao, Z.; Cao, X.; Xia, X.G.; Schober, R. Millimeter-wave full-duplex UAV relay: Joint positioning, beamforming, and power control. *IEEE J. Sel. Areas Commun.* **2020**, *38*, 2057–2073. [CrossRef]
9. Mohapatra, A.; Trinh, T. Early wildfire detection technologies in practice—A review. *Sustainability* **2022**, *14*, 12270. [CrossRef]
10. Javaid, S.; Saeed, N.; Qadir, Z.; Fahim, H.; He, B.; Song, H.; Bilal, M. Communication and Control in Collaborative UAVs: Recent Advances and Future Trends. *IEEE Trans. Intell. Transp. Syst.* **2023**, *24*, 5719–5739. [CrossRef]
11. Bushnaq, O.M.; Chaaban, A.; Al-Naffouri, T.Y. The role of UAV-IoT networks in future wildfire detection. *IEEE Internet Things J.* **2021**, *8*, 16984–16999. [CrossRef]
12. Yang, J.; Qian, J.; Gao, H. Forest wildfire monitoring and communication uav system based on particle swarm optimization. *J. Physics: Conf. Ser.* **2021**, *1982*, 012068. [CrossRef]
13. Umunnakwe, A.; Davis, K. An Optimization of UAV-Based Remote Monitoring for Improving Wildfire Response in Power Systems. *IEEE Open Access J. Power Energy* **2023**, *10*, 678–688. [CrossRef]
14. Rjoub, D.; Alsharoa, A.; Masadeh, A. Unmanned-Aircraft-System-Assisted Early Wildfire Detection with Air Quality Sensors. *Electronics* **2023**, *12*, 1239. [CrossRef]
15. Phan, C.; Liu, H.H. A cooperative UAV/UGV platform for wildfire detection and fighting. In Proceedings of the 2008 Asia Simulation Conference-7th International Conference on System Simulation and Scientific Computing, Beijing, China, 10–12 October 2008; IEEE: Piscataway, NJ, USA, 2008; pp. 494–498.
16. Qiao, L.; Li, S.; Zhang, Y.; Yan, J. Early Wildfire Detection and Distance Estimation Using Aerial Visible-Infrared Images. *IEEE Trans. Ind. Electron.* **2024**, 1–11. [CrossRef]
17. Bashir, M.H.; Ahmad, M.; Rizvi, D.R.; El-Latif, A.A.A. Efficient CNN-based disaster events classification using UAV-aided images for emergency response application. *Neural Comput. Appl.* **2024**, *36*, 10599–10612. [CrossRef]
18. Chen, X.; Xiao, Z.; Cheng, Y.; Hsia, C.; Wang, H.; Xu, J.; Xu, S.; Dang, F.; Zhang, X.P.; Liu, Y.; et al. SOScheduler: Toward Proactive and Adaptive Wildfire Suppression via Multi-UAV Collaborative Scheduling. *IEEE Internet Things J.* **2024**, *11*, 24858–24871. [CrossRef]
19. Lewicki, T.; Liu, K. Multimodal wildfire surveillance with uav. In Proceedings of the 2021 IEEE Global Communications Conference (GLOBECOM), Madrid, Spain, 7–11 December 2021; pp. 1–6.
20. Ali, M.F.; Jayakody, D.N.K. SIMO-underwater visible light communication (UVLC) system. *Comput. Netw.* **2023**, *232*, 109750.
21. Aggarwal, M.; Garg, P.; Puri, P. Analysis of subcarrier intensity modulation-based optical wireless DF relaying over turbulence channels with path loss and pointing error impairments. *IET Commun.* **2014**, *8*, 3170–3178. [CrossRef]
22. Miglani, R.; Malhotra, J.S. Performance enhancement of high-capacity coherent DWDM free-space optical communication link using digital signal processing. *Photonic Netw. Commun.* **2019**, *38*, 326–342. [CrossRef]
23. Elamassie, M.; Miramirkhani, F.; Uysal, M. Channel modeling and performance characterization of underwater visible light communications. In Proceedings of the 2018 IEEE International Conference on Communications Workshops (ICC Workshops), Kansas City, MO, USA, 20–24 May 2018; pp. 1–5.
24. Ali, M.F.; Jayakody, D.N.K.; Garg, S.; Kaddoum, G.; Hossain, M.S. Dual-Hop Mixed FSO-VLC Underwater Wireless Communication Link. *IEEE Trans. Netw. Serv. Manag.* **2022**, *19*, 3105–3120. [CrossRef]
25. Zedini, E.; Ata, Y.; Alouini, M.S. Improving Performance of Integrated Ground-HAPS FSO Communication Links with MIMO Application. *IEEE Photonics J.* **2024**, *16*, 7301214. [CrossRef]
26. Elahee, M.N.; Faisal, M. Performance Analysis of Terrestrial FSO Communication Under Typical Rain-Affected Environment of Bangladesh. In Proceedings of the 2024 International Conference on Advances in Computing, Communication, Electrical, and Smart Systems (iCACCESS), Dhaka, Bangladesh, 8–9 March 2024; pp. 1–6.
27. Xu, G.; Zhang, N.; Xu, M.; Xu, Z.; Zhang, Q.; Song, Z. Outage Probability and Average BER of UAV-assisted Dual-hop FSO Communication with Amplify-and-Forward Relaying. *IEEE Trans. Veh. Technol.* **2023**, *72*, 8287–8302. [CrossRef]
28. Xu, Z.; Xu, G.; Zheng, Z. BER and channel capacity performance of an FSO communication system over atmospheric turbulence with different types of noise. *Sensors* **2021**, *21*, 3454. [CrossRef] [PubMed]

29. Varotsos, G.; Stassinakis, A.; Nistazakis, H.; Tsigopoulos, A.; Peppas, K.; Aidinis, C.; Tombras, G. Probability of fade estimation for FSO links with time dispersion and turbulence modeled with the gamma–gamma or the IK distribution. *Opt.-Int. J. Light Electron Opt.* **2014**, *125*, 7191–7197. [CrossRef]
30. Lionis, A.; Peppas, K.; Nistazakis, H.E.; Tsigopoulos, A.; Cohn, K.; Drexler, K.R. Supervised Machine Learning for Refractive Index Structure Parameter Modeling. *Quantum Beam Sci.* **2023**, *7*, 18. [CrossRef]
31. Wolfram Mathematical. Available online: http://functions.wolfram.com/01.06.02.0001.01 (accessed on 1 September 2023).
32. Wolfram Mathematical. Available online: https://meteostat.net/en/place/pt/alfragide?s=08535&t=2023-07-22/2023-07-29 (accessed on 1 September 2023).
33. Tsiftsis, T.A.; Sandalidis, H.G.; Karagiannidis, G.K.; Uysal, M. Optical wireless links with spatial diversity over strong atmospheric turbulence channels. *IEEE Trans. Wirel. Commun.* **2009**, *8*, 951–957. [CrossRef]

Disclaimer/Publisher's Note: The statements, opinions and data contained in all publications are solely those of the individual author(s) and contributor(s) and not of MDPI and/or the editor(s). MDPI and/or the editor(s) disclaim responsibility for any injury to people or property resulting from any ideas, methods, instructions or products referred to in the content.